Template Synthesis of Amorphous $NiFeCuO_x$ Arrays for Efficient Anion-Exchange Membrane Water Oxidation

Qilong Liu[1†], Cheng Gong[1†], Xiaole Zhang[1], Peng Chen[1], Mengxiang Wang[2], Qizhu Qian[2], Jujia Zhang[1], Mingliang Fang[1*], and Wentuan Bi[1*]

[1] Institute of Energy, Hefei Comprehensive National Science Center (Anhui Energy Laboratory), Hefei, Anhui, 230031, P. R. China

[2] Hefei National Research Center for Physical Sciences at the Microscale, University of Science and Technology of China, Hefei, Anhui, 230026, P. R. China

* Represents the corresponding author

† Represent contribution equality to this work.

Chemicals

Ammonium persulfate ($(NH_4)_2S_2O_8$, AR, ≥98.5%), sodium hydroxide (NaOH, AR, ≥96.0%), oxalic acid dihydrate ($H_2C_2O_4·2H_2O$, AR, ≥99.5%), nickel chloride hexahydrate ($NiCl_2·6H_2O$, AR, ≥98.0%), ferrous chloride tetrahydrate ($FeCl_2·4H_2O$, AR, ≥99.0%), copper foam (1.5 mm in thickness, 99.9% purity), and potassium hydroxide (KOH, AR, ≥85.0%) were purchased from Sinopharm Chemical Reagent Co., Ltd. All reagents were used without further purification. The distilled water employed in all experiments was purified using a Millipore system (18.25 MΩ·cm).

Materials Synthesis

Synthesis of Cu(OH)/CuF: Firstly, the cut copper foam (3×4 cm，CuF) was sequentially immersed in 10-fold diluted hydrochloric acid solution and anhydrous ethanol for 10 min under ultrasonication to remove surface oxides and contaminants. Then, 10 mL of 0.125 M $(NH_4)_2S_2O_8$ solution and 10 mL of 1 M NaOH solution were prepared and mixed uniformly. Subsequently, the cleaned copper foam was vertically placed in the mixed solution for 20 min, then taken out, rinsed several times with water and anhydrous ethanol, and dried to obtain the $Cu(OH)_2$/CuF precursor.

Synthesis of NiFeCu oxalic /CuF：A 20 mL solution containing 50 mM oxalic acid, X mM $NiCl_2 · 6H_2O$ (X=50,45,40,35,30,25), and (50-X) mM $FeCl_2·4H_2O$ was prepared. The $Cu(OH)_2$/CuF was then vertically immersed in the solution for 1 h, taken out, rinsed several times with water and anhydrous ethanol, and dried to obtain NiFeCu oxalate/CuF.

Synthesis of $NiFeCuO_x$ array /CuF and control electrodes: A three-electrode system was employed, with 1 M KOH as the electrolyte. Herein, NiFeCu oxalate/CuF served as the working electrode, Hg/HgO as the reference electrode, and a graphite rod as the counter electrode. CV activation was conducted within the voltage range of 0-0.9 V vs. Hg/HgO. LSV measurements indicated that the working electrode prepared at X=30 exhibited the best performance, which was designated as NiFeCuOx array/CuF. The activated electrode obtained at X=50 was designated as NiCuOx array/CuF. The sample

obtained by directly immersing CuF in the mixed solution of metals and oxalic acid, followed by activation, was designated as NiFeOx no array/CuF.

Characterizations

The X-ray diffraction (XRD) patterns were recorded on a Philips X'Pert Pro Super diffractometer with Cu Kα radiation (λ = 1.54178 Å) at a speed of 35° in a 2θ range of 10-80°. The Scanning electron microscopy (SEM) images were performed by GeminiSEM 450. The transmission electron microscopy (TEM) images, high-resolution TEM (HR-TEM), and energy-dispersive X-ray Spectroscopy (EDS) element mapping were taken on JEOL-2100F with an accelerating voltage of 200 kV. The X-ray photoelectron spectroscopy (XPS) spectra were collected on Thermo Scientific K-Alpha spectrometer. The in-situ Raman spectra were measured using an Xplora Plus confocal microprobe Raman system (HORIBA) with 1200 T grating. The excitation laser was a He-Ne laser with a wavelength of 532 nm. A ×50 magnification long working distance (8 mm) objective was used and it took approximately 120 s to acquire one experimental Raman spectrum with two accumulations. The Raman frequencies were calibrated using a Si wafer (520.7 cm^{-1}) before the experiment. Linear sweep voltammetry (LSV) curves were tested using CHI 760e workstation. Electrochemical impedance spectroscopy (EIS) and electrochemical stability tests were performed using a CS310M electrochemical workstation (Wuhan CorrTest Instrument Co., Ltd.).

Electrochemical measurements

The electrochemical performance was evaluated using a three-electrode system in 1 M KOH solution. The synthesized catalysts served as the working electrode, with a graphite counter electrode and a Hg/HgO reference electrode. A single electrolytic cell was utilized for the experiments. Linear sweep voltammetry (LSV) tests were conducted at a scan rate of 5 mV s^{-1}. Electrochemical impedance spectroscopy (EIS) measurements were recorded from 100 kHz to 0.05 Hz with a 5 mV amplitude. The

potential relative to the Hg/HgO electrode was converted to that of the standard reversible hydrogen electrode (RHE) using the equation:

$$V\ (\text{vs. RHE}) = V\ (\text{vs. Hg/HgO}) + 0.059 \times \text{pH} + 0.098$$

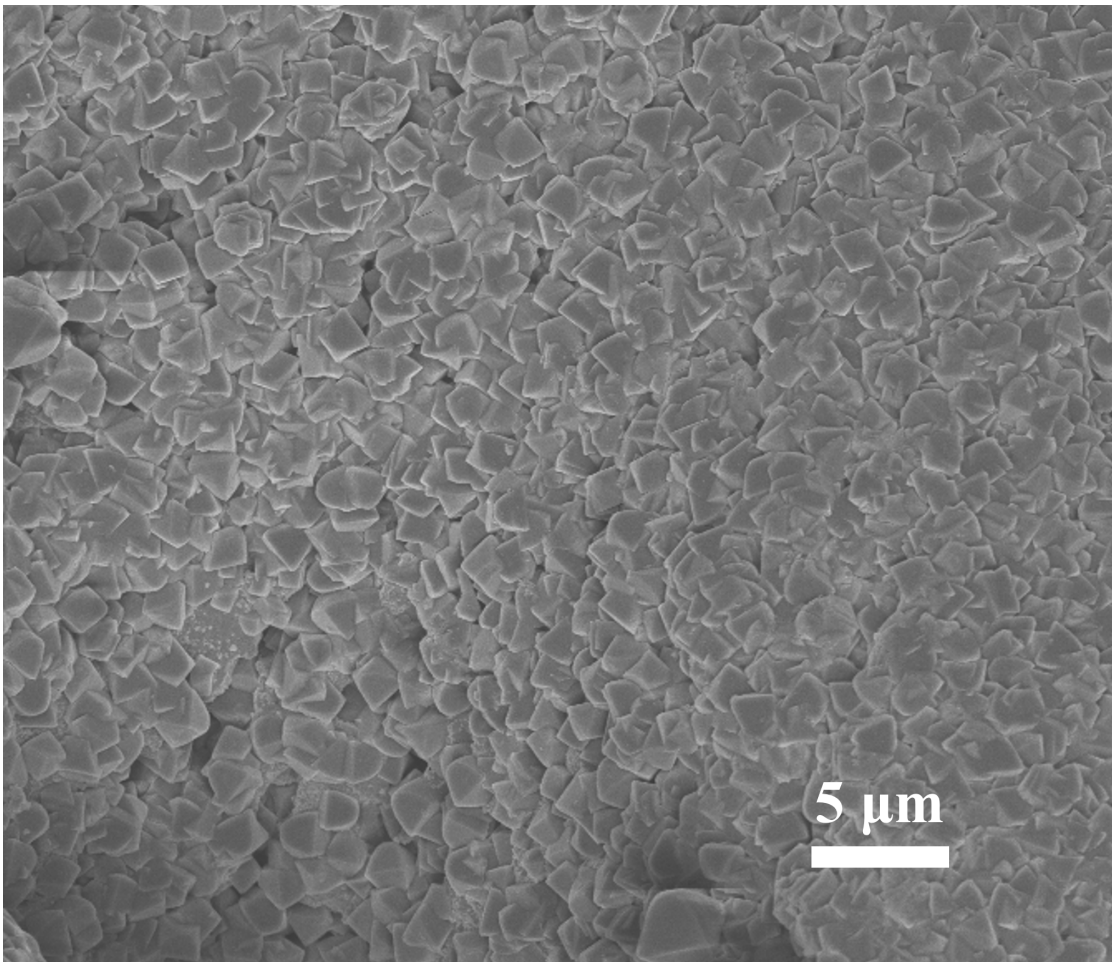

Figure S 1 SEM image of NiFe oxalate without array structure.

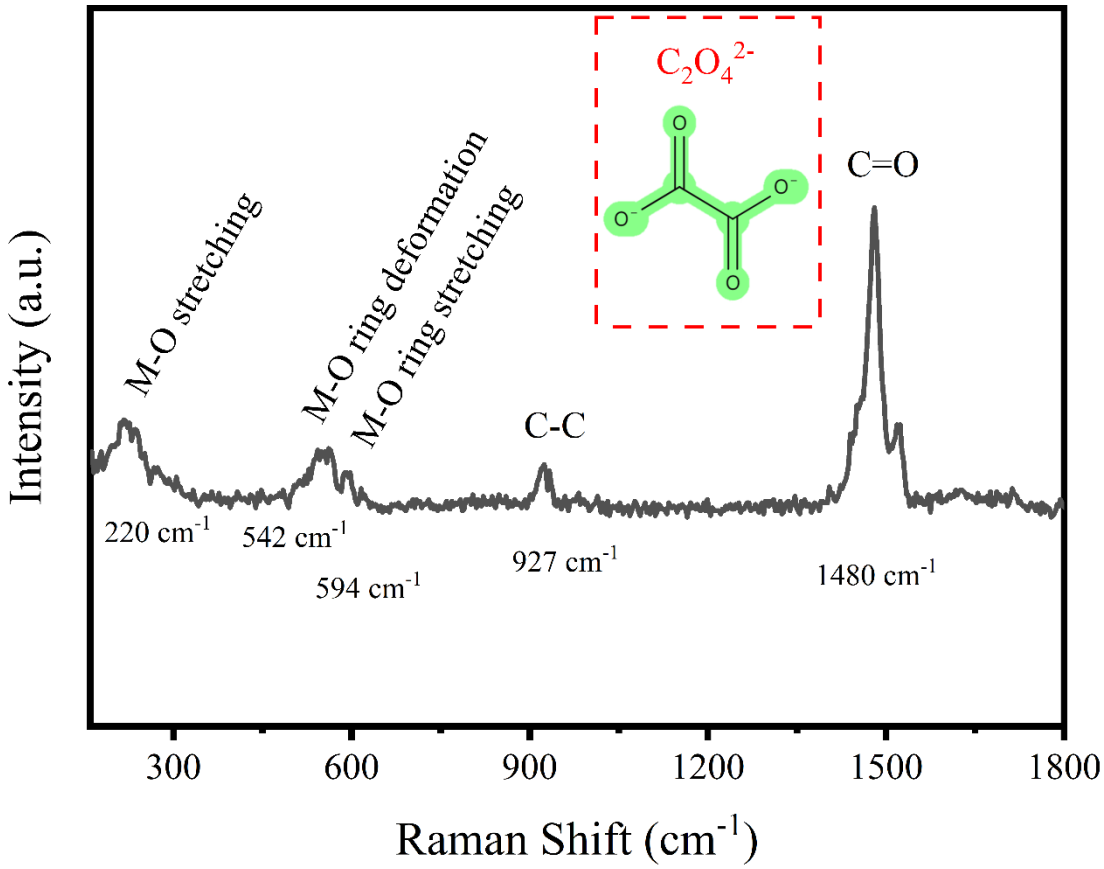

Figure S 2 Raman spectrum of NiFeCu oxalate compound.

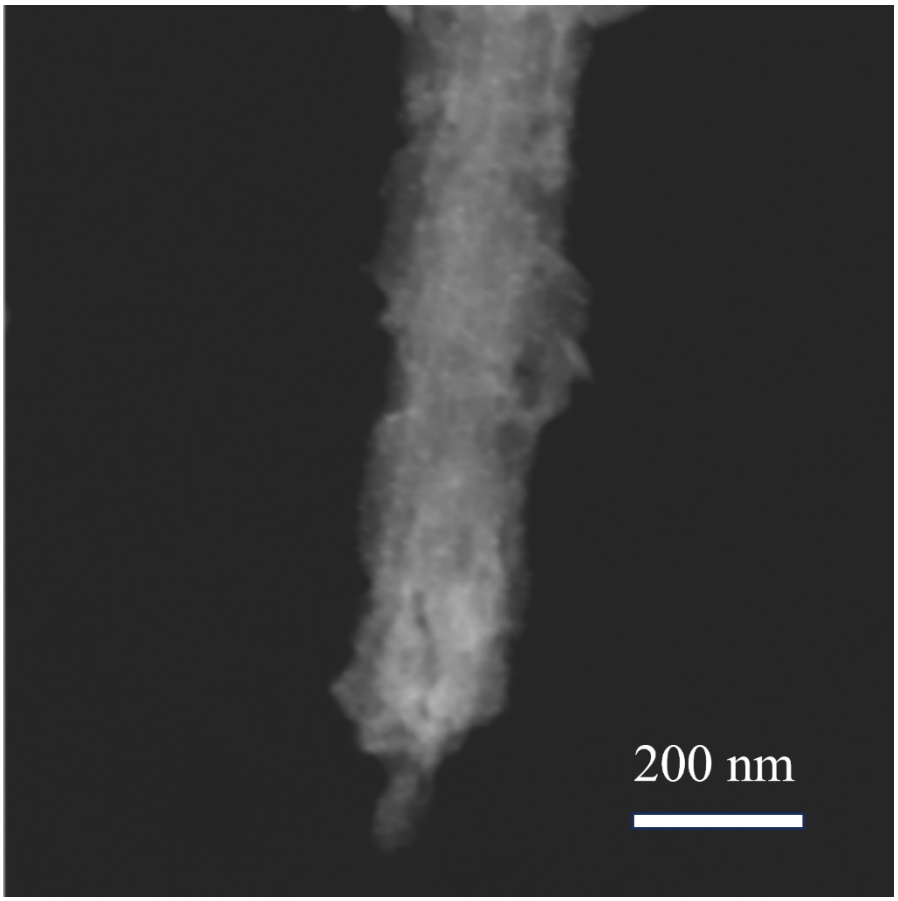

Figure S 3 TEM image of the $NiFeCuO_x$ nanorod.

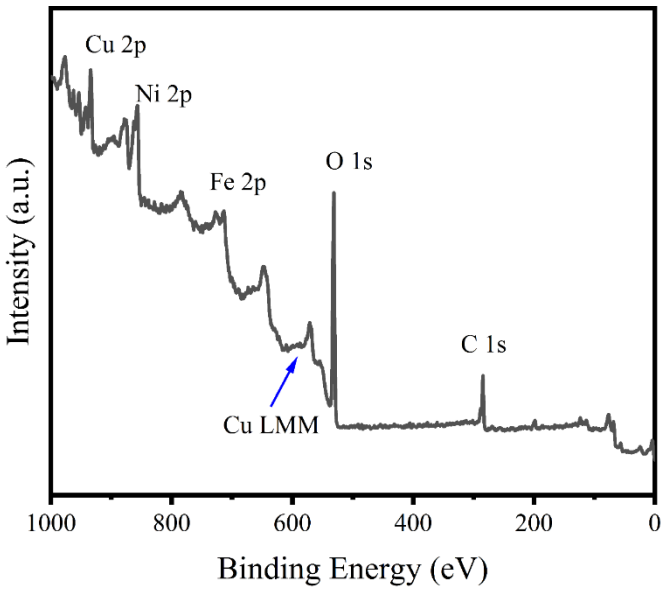

Figure S 4 The survey XPS of the $NiFeCuO_x$/CuF.

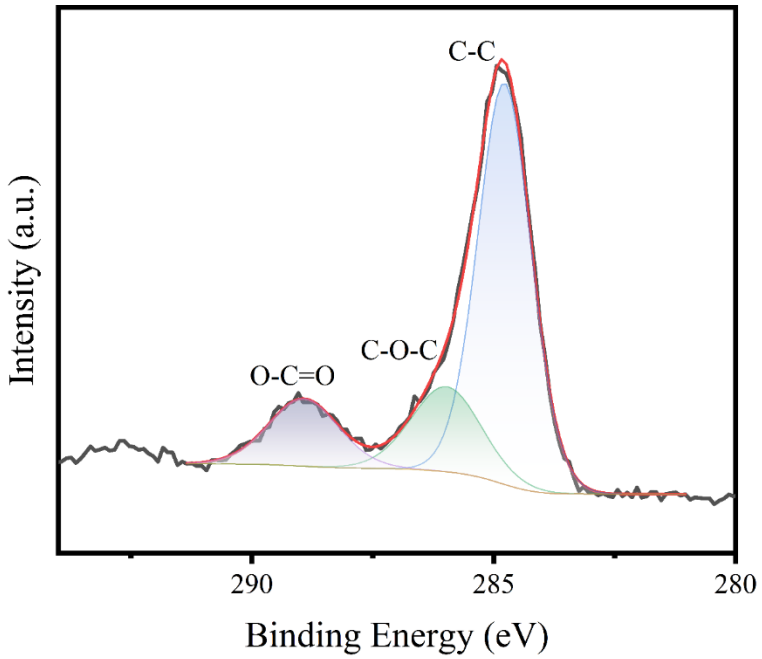

Figure S 5 The high-resolution XPS spectrum of C 1s from $NiFeCuO_x$ array/CuF.

Table S 1 The atomic contents of Fe 3p and Ni 3p.

Name	BE	FWHM	Atomic conc.
Fe 3p	56.74	3.20	39.9
Ni 3p	67.94	2.87	60.1

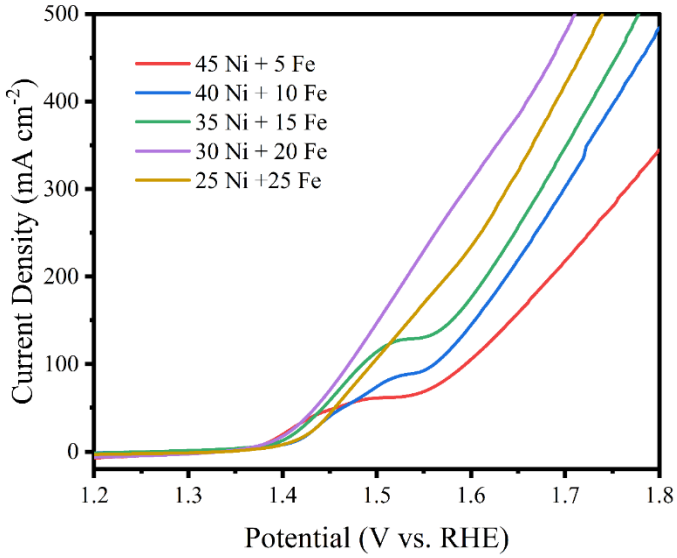

Figure S 6 The LSV curves of electrodes with different NiFe ratios.

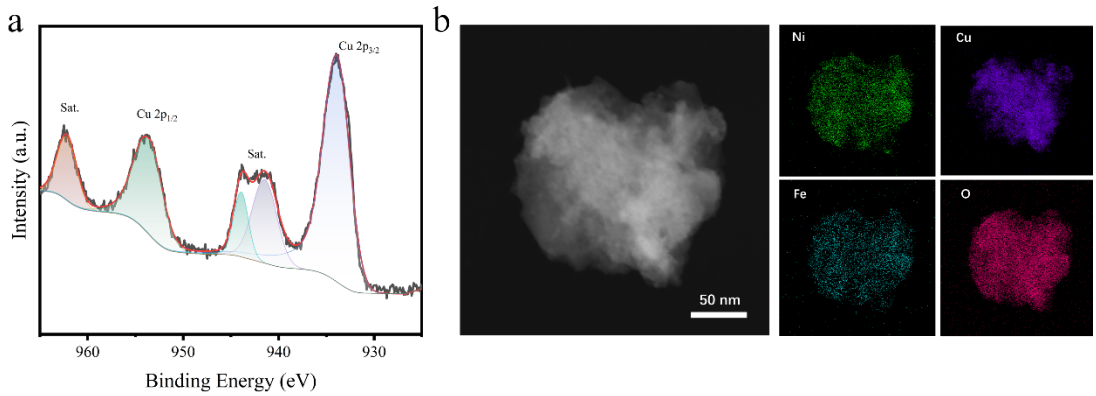

Figure S 7 (a) The high-resolution XPS spectrum of Cu 2p from $NiFeCuO_x$ no array/CuF. (b) EDS mapping of active species sonication detached from $NiFeCuO_x$ no array/CuF.

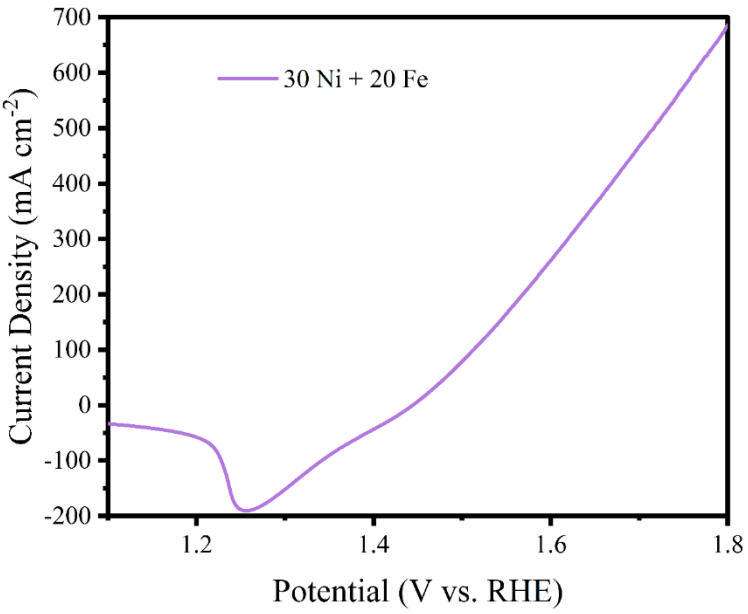

Figure S 8 The reverse LSV curve of the $NiFeCuO_x$ array/CuF.

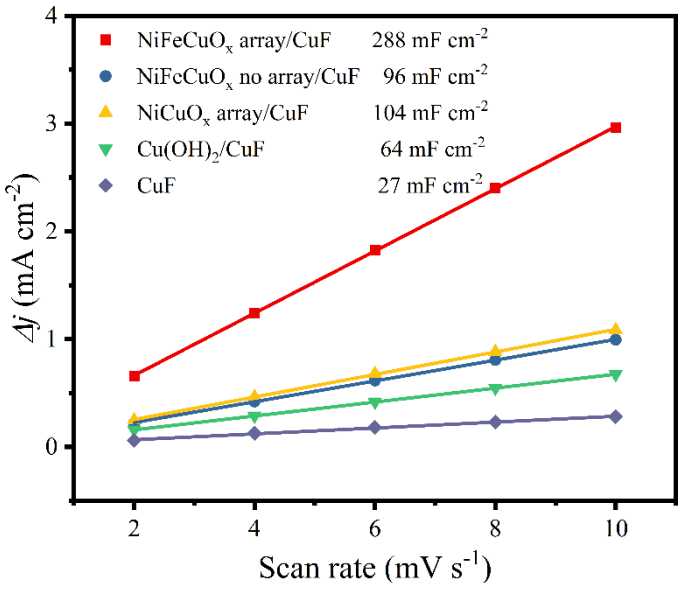

Figure S 9 C_{dl} of the electrodes.

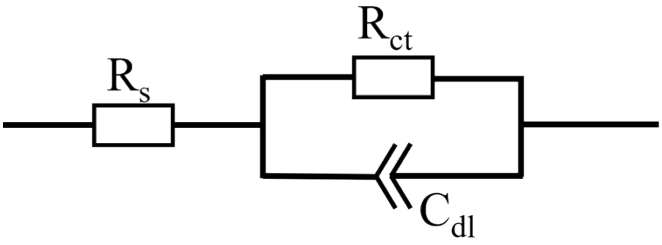

Figure S 10 The equivalent circuit of EIS.

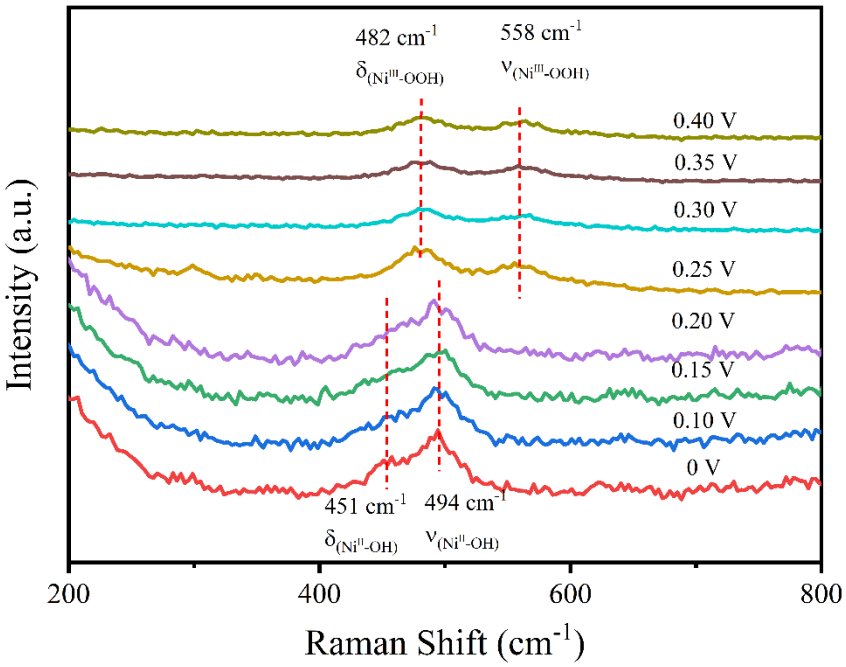

Figure S 11 In-situ Raman spectra of $NiCuO_x$ array/CuF during OER.

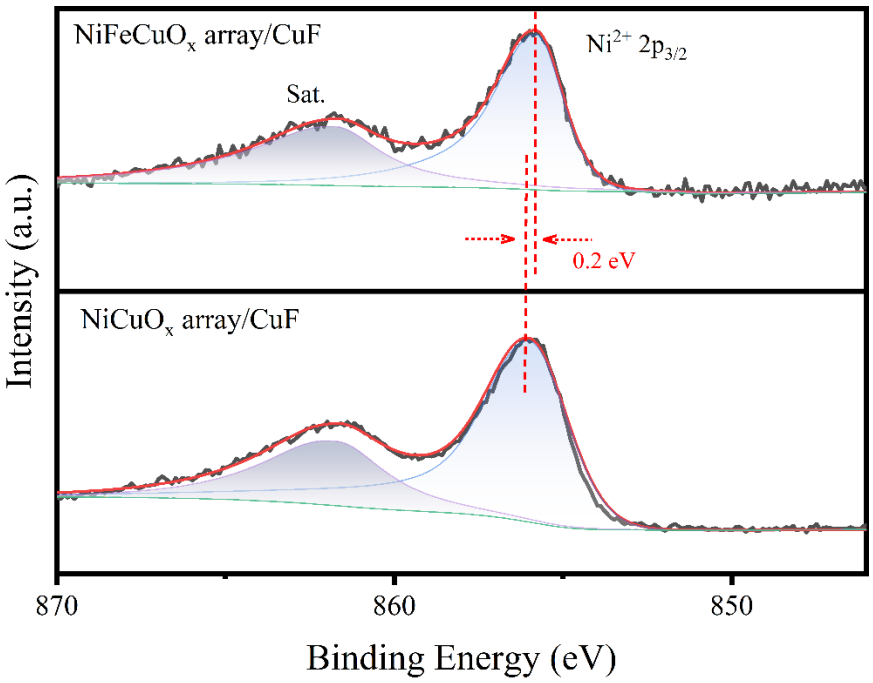

Figure S 12 The high-resolution XPS spectra of Ni $2p_{3/2}$ from $NiFeCuO_x$ array/CuF and $NiCuO_x$ array/CuF.

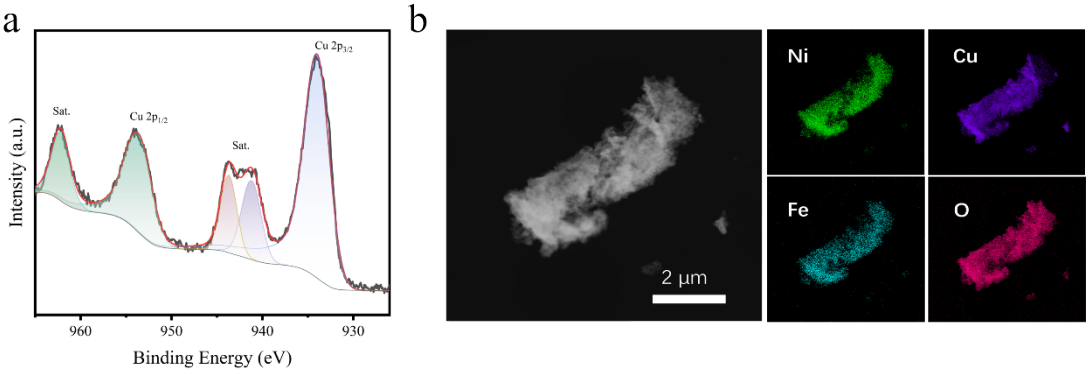

Figure S 13 (a) The high-resolution XPS spectrum of Cu 2p from $NiFeCuO_x$ array/CuF after stability test. (b) the EDS mapping of the $NiFeCuO_x$ species after stability test.

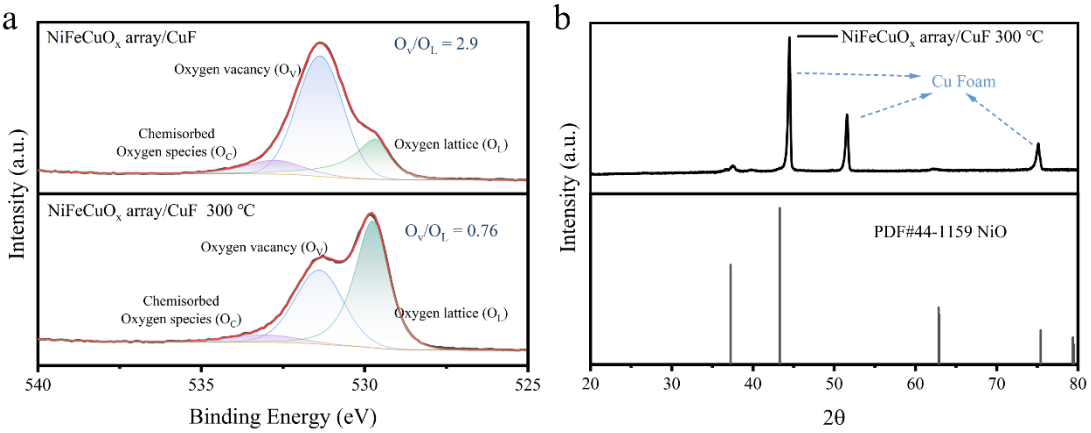

Figure S 14 (a) The high-resolution XPS spectra of O 1s from $NiFeCuO_x$ array/CuF and $NiFeCuO_x$ array/CuF 300 ℃. (b) the XRD pattern of $NiFeCuO_x$ array/CuF 300 ℃.

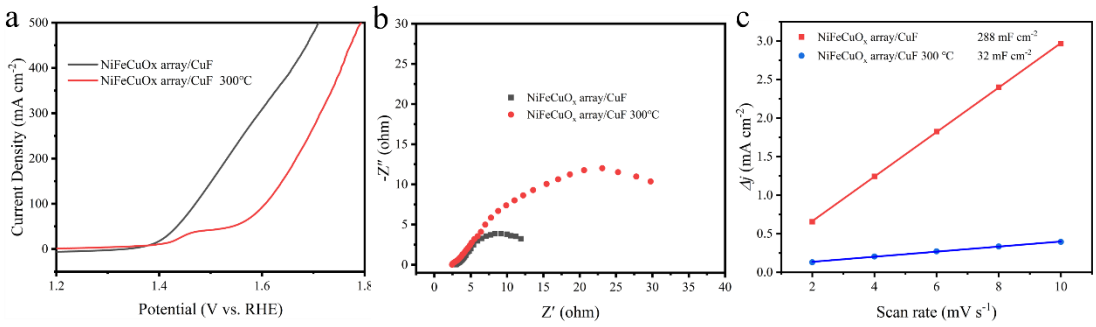

Figure S 15 (a) LSV curves,(b) EIS, (c) C_{dl} of $NiFeCuO_x$ array/CuF and $NiFeCuO_x$ array/CuF 300 ℃.

Table S 2 Comparison of OER performance for different materials.

Catalysts	Overpotential (mV@ mA cm^{-2})	Tafel slop (mV dec^{-1})	Ref.
$NiFeCuO_x$ array/CuF	283 mV @ 100 mA cm-2	71	This work
NiMOF/BP	260 mV @ 10 mA cm-2	76	1
Dy@Ni-MOF	246 mV @ 10 mA cm-2	96	2
Ni/MnO@N-C NS/NFs	306 mV @ 10 mA cm-2	91.2	3
Tan-CN-NiFe	320 mV @ 10 mA cm-2	58	4
DS-CeO_2/NiCo LDH	282 mV @ 10 mA cm-2	82	5
Co_3Fe_1 MOF-Py3	269 mV @ 10 mA cm-2	45	6
S-Ni-MOF/Fe-MOF	224 mV @ 10 mA cm-2 281mV @ 100 mA cm-2	56.3	7
FeCoNo-hydroxide	212 mV @ 10 mA cm-2 319 mV @ 100 mA cm-2	52	8
Ni_3S_2-P	420 mV @ 100 mA cm-2	224	9
3D Phosphorylated NiFe hydroxide	290 mV @ 10 mA cm-2	38	10
3D Ni-Fe oxides/(oxy)hydroxides	232 mV @ 10 mA cm-2 280 mV @ 100 mA cm-2	51	11

Table S 3 the Cu 2p/Ni 2p radio of $NiFeCuO_x$ array/CuF and $NiFeCuO_x$ no array/CuF.

Electrodes	Cu 2p (At. %)	Ni 2p (At. %)	Cu 2p/Ni 2p
$NiFeCuO_x$ array/CuF	14.83	4.75	3.12
$NiFeCuO_x$ no array/CuF	8.29	8.53	0.97

Table S 4 Comparison of the AEM water electrolyzer performance of other work.

	Anode	Cathode	AEM performance	Ref.
1	NiFeCuOx array/CuF	Pt/C	2.7 A cm^{-2}@2 V	This Work
2	CoOOH	Pt/C	3.4 A cm^{-2}@2 V	12
3	NiFeMn@triMPi	Pt/C	2.8 A cm^{-2}@2 V	13
4	$Co_{0.75}Fe_{0.25}PO_x$ /NF	Pt/C	3.47 A cm^{-2}@2 V	14
5	FAA/PTFE	Pt/C	2.9 A cm^{-2}@2 V	15
6	Fe-Ni_2P/$NiMoO_4$	$MoNi_4$	1 A cm^{-2}@2.18 V	16
7	F-TMO	Pt black	3 A cm^{-2}@2.56 V	17
8	z-NiFe	$MoNi_4/MoO_2$	1 A cm^{-2}@1.76 V	18
9	NiFeCoLi/NF	Pt/C/CP	2 A cm^{-2}@1.9 V	19
10	Ir_{sac}-NiFe LDH/NF	Pt/C/CP	1 A cm^{-2}@1.73 V	20
11	Fe_2O_3@CeO_2–O_V	Pt/C	1 A cm^{-2}@1.93 V	21
12	NDCO	Pt/C	1 A cm^{-2}@1.78 V	22
13	Fe-Co_3-Ni	Pt/C	2 A cm^{-2}@1.89 V	23
14	$Co_2FeW_{1.6}O_x$	Pt/C	1 A cm^{-2}@1.69 V	24

1. W. Zhai, Y. Chen, Y. Liu, T. Sakthivel, Y. Ma, Y. Qin, Y. Qu and Z. Dai, Enlarging the Ni–O Bond Polarizability in a Phosphorene-Hosted Metal–Organic Framework for Boosted Water Oxidation Electrocatalysis, *ACS Nano*, 2023, **17**, 17254-17264.
2. Z. Huang, M. Liao, S. Zhang, L. Wang, M. Gao, Z. Luo, T. T. Isimjan, B. Wang and X. Yang, Valence electronic engineering of superhydrophilic Dy-evoked Ni-MOF outperforming RuO2 for highly efficient electrocatalytic oxygen evolution, *Journal of Energy Chemistry*, 2024, **90**, 244-252.
3. C. Ge, Z.-J. Li, Y.-N. Chang, T.-F. Li, B. He, T.-Y. Lu and L. Xu, The manipulation of Ni/MnO heterostructures within carbon hierarchical superstructures as bifunctional oxygen electrocatalysts for enhanced Zn–air batteries, *Rare Metals*, 2025, **44**, 3107-3118.
4. W. Wan, L. Kang, A. Schnegg, O. Ruediger, Z. Chen, C. S. Allen, L. Liu, S. Chabbra, S. DeBeer and S. Heumann, Carbon-Supported Single Fe/Co/Ni Atom Catalysts for Water Oxidation: Unveiling the Dynamic Active Sites, *Angewandte Chemie International Edition*, 2025, **64**, e202424629.
5. L. Guo, Z. Zhang, Z. Mu, P. Da, L. An, W. Shen, Y. Hou, P. Xi and C.-H. Yan, Ceria-Optimized Oxygen-Species Exchange in Hierarchical Bimetallic Hydroxide for Electrocatalytic Water Oxidation, *Advanced Materials*, 2024, **36**, 2406682.
6. Y. Liu, S. Deng, S. Fu, X. Wang, G. Liu and H. Yang, Pyridine-induced caused structural reconfiguration forming ultrathin 2D metal–organic frameworks for the oxygen evolution reaction, *Journal of Materials Chemistry A*, 2024, **12**, 8885-8892.
7. H. Ru, Y. Bao, Y. Wang, X. Wang, J. Tu, Q. Wu, Y. Li and L. Ding, S2−-modified hetero MOF-on-MOF of Ni-MOF/Fe-MOF with efficient seawater oxidation performance, *Journal of Alloys and Compounds*, 2024, **1007**, 176164.
8. Q. Liu, H. Zhang, J. Xu, L. Wei, Q. Liu and X. Kong, Facile Preparation of Amorphous Fe–Co–Ni Hydroxide Arrays: A Highly Efficient Integrated Electrode for Water Oxidation, *Inorganic Chemistry*, 2018, **57**, 15610-15617.
9. Q. Liu, L. Wei, Q. Liu, G. Chen and X. Kong, Anion Engineering on 3D Ni3S2 Nanosheets Array toward Water Splitting, *ACS Applied Energy Materials*, 2018, **1**, 3488-3496.
10. Y. Li and C. Zhao, Enhancing Water Oxidation Catalysis on a Synergistic Phosphorylated NiFe Hydroxide by Adjusting Catalyst Wettability, *ACS Catalysis*, 2017, **7**, 2535-2541.
11. J. Shen, M. Wang, L. Zhao, J. Jiang, H. Liu and J. Liu, Self-Supported Stainless Steel Nanocone Array Coated with a Layer of Ni–Fe Oxides/(Oxy)hydroxides as a Highly Active and Robust Electrode for Water Oxidation, *ACS Applied Materials & Interfaces*, 2018, **10**, 8786-8796.
12. J. Zhao, K. Wang, X. Li, X. Li, X. Cui and X. Zhao, Localizing the Long-Range Disorder of Reconstructed Cobalt Oxyhydroxides for Anion Exchange Membrane Water Electrolysis, *Angewandte Chemie International Edition*, 2025, **64**, e202513592.
13. X. Jiang, Q. Yu, Z. Wen, L. Fan, W. Li, J. Fan and H. Li, Structural Engineering of Crystalline–Amorphous NiFeMn Alloy and Trimetallic Phosphite Heterostructure Electrocatalysts for High-Performance Industrial Anion Exchange

Membrane Water Electrolysis, *ACS Applied Materials & Interfaces*, 2025, **17**, 63296-63307.
14. Y. Gao, A. Yu, C. Sun, D. Li, C. Zhang and H. Lv, Engineering delocalized electron and spin states via Fe/O dual-doping in CoP Nanorod arrays for high-efficiency oxygen evolution reaction, *Chemical Engineering Journal*, 2025, **522**, 167287.
15. K. W. Kim, K. A. Lee, J. H. Lee, S. H. Kim, J. F. Kim, T. H. Kim, S. Kim, Y.-E. Sung and K. R. Yoon, Membrane Reinforcement Strategy Using Robust Nanofibers for Durable and Safe AEM Water Electrolysis, *Small*, 2025, **21**, e04805.
16. X. Tao, L. Hou, X. Wang, J. Jin, H. Li and F. Gao, Iron and oxygen vacancies co-modulated adsorption evolution and lattice oxygen dual-path mechanism for water oxidation, *Nature Communications*, 2025, **16**, 8788.
17. L. Zhang, Q. Xu, S. Wen, H. Zhang, L. Chen, H. Jiang and C. Li, Recycling Spent Ternary Cathodes to Oxygen Evolution Catalysts for Pure Water Anion-Exchange Membrane Electrolysis, *ACS Nano*, 2024, **18**, 22454-22464.
18. W. Li, Y. Ding, Y. Zhao, Z. Li, G. Lin, L. Wang and L. Sun, Zwitterion-Modified NiFe OER Catalyst Achieving Ultrastable Anion Exchange Membrane Water Electrolysis via Dynamic Alkaline Microenvironment Engineering, *Angewandte Chemie International Edition*, 2025, **64**, e202505924.
19. L. Cong, C. Tang, X. Li, W. He, C. Wang, E. Angelica and Q. Zhang, Li-Doping and Pyrolysis Engineered Robust Anode for Intermittency-Resilient AEM Electrolysis, *Advanced Energy Materials*, 2025, **15**, e04707.
20. Z. Duan, Z. Cui, Z. Gao, W. Xu, Y. Liang, H. Jiang, Z. Li, F. Wang and S. Zhu, Single-Atom Iridium Orchestrates a Reaction Pathway Shift to Activate Lattice Oxygen for Efficient Oxygen Evolution, *ACS Catalysis*, 2025, **15**, 16882-16892.
21. Q. Huang, G.-J. Xia, B. Huang, D. Xie, J. Wang, D. Wen, D. Lin, C. Xu, L. Gao, Z. Wu, J. Wu, F. Xie, W. Guo and R. Zou, Activating lattice oxygen by a defect-engineered Fe2O3–CeO2 nano-heterojunction for efficient electrochemical water oxidation, *Energy & Environmental Science*, 2024, **17**, 5260-5272.
22. P.-C. Yu, X.-L. Zhang, T.-Y. Zhang, X.-Y.-N. Tao, Y. Yang, Y.-H. Wang, S.-C. Zhang, F.-Y. Gao, Z.-Z. Niu, M.-H. Fan and M.-R. Gao, Nitrogen-Mediated Promotion of Cobalt-Based Oxygen Evolution Catalyst for Practical Anion-Exchange Membrane Electrolysis, *Journal of the American Chemical Society*, 2024, **146**, 20379-20390.
23. C. Lee, Y. H. Yun, S.-H. Kim, G. Doo, S. Lee, H. Park, Y. Park, J. Shin, H.-S. Cho, S.-K. Kim, E. Cho, C. Jung and M. Kim, Structural and Compositional Optimization of Fe–Co–Ni Ternary Amorphous Electrocatalysts for Efficient Oxygen Evolution in Anion Exchange Membrane Water Electrolysis, *Small*, 2025, **21**, 2405468.
24. G. Gao, G. Li, T. Huang, J. Wan, Z. Geng, H. Tang, X. Zhao, S. Fu, L. Sun, J. Li and L. Li, Overcoming the Activity-Stability Trade-Off in Electrocatalysts via Unconventional Two-Step Structural Reconstructions of Amorphous Oxides, *Journal of the American Chemical Society*, 2025, **147**, 29767-29778.